Infrared Radiation from H_2O, CO_2, or NH_3 Collisionally Excited by N_2, O, or Ar

M. G. DUNN,* G. T. SKINNER,† AND C. E. TREANOR‡
Calspan Corporation, Buffalo, N.Y.

Results are reported of an experimental study to elicit the spectral infrared radiative properties of H_2O, CO_2, or NH_3 molecules that have been involved in a single high-energy collision with N_2, O, or argon. A pressure-driven reflected-shock tunnel was used to produce a 5.8 km/sec supply of N_2 molecules or a 4.3 km/sec supply of O atoms or a 5.4 km/sec supply of argon that subsequently impacted the target molecules. Experimental values of σ_*/τ (excitation cross section/radiative lifetime) are presented for the wavelength regions 2.5–3.1 μm, 5.7–7.5 μm, 8.3–9.2 μm, 9.1–10.3 μm, 10.6–11.6 μm, 11.1–14.0 μm, and 8.3–14.0 μm for the N_2-H_2O collisions. Values of σ_*/τ are also presented for the N_2-CO_2 collisions in the wavelength regions 4.28–4.34 μm, 8.3–9.2 μm, 9.1–10.3 μm, 10.6–11.6 μm, and 8.3–14.0 μm. In addition, values of σ_*/τ are reported for the N_2-NH_3 interaction in the wavelength intervals 8.3–9.2 μm, 10.6–11.6 μm, and 8.3–14.0 μm. Experimental values of σ_*/τ are also presented for the O-H_2O interaction in the wavelength intervals 2.46–3.13 μm, 5.67–7.45 μm, and 11.1–14.0 μm. A value of σ_*/τ is given for Ar-H_2O collisions at 5.4 km/sec in the wavelength interval 5.67–7.45 μm. These experimental values of σ_*/τ are compared with theoretical calculations of the effective values of σ_*/τ for radiation in the given wavelength intervals. Using available values of the radiative lifetimes, values for σ_* were obtained.

Nomenclature

a = y coordinate of the lower flat plate
A_d = area of infrared detector
A_j = Einstein coefficient for spontaneous emission
h = distance between the flat plates
n_1 = number density of the incident stream
$n_2(y)$ = number density of the target stream
P = maximum collision probability of collision for an incident stream particle with the target stream
P_R = probability of excitation of a given rotational state
P_v = probability of excitation of a given vibrational state
v_1 = velocity of the incident stream
v_2 = velocity of the target stream
v_* = velocity of the center of mass in an incident-target molecule collision
w = total flux of photons into detector (photons sec^{-1})
x = coordinate parallel to the incident stream
y = coordinate parallel to the axis of the target stream
z = coordinate at right angles to x and to y
ξ = y/η
η = $v_2/(v_1 n_1 \sigma_0)$
θ = apex angle of the target and field-of-view cones
$\overline{\theta}_j$ = defined by Eq. (12)
λ = wavelength
$\Delta\lambda$ = wavelength interval
σ_0 = elastic collision cross section for the incident stream particle and the target gas
σ_{vR} = cross section for excitation to the v, R vibrational-rotational state
σ_* = collision cross section for a participating excited state
τ = lifetime of a participating excited state
$\psi_2(y)$ = total flux of target molecules at height y (molecules sec^{-1})
$(\ )_1$ = pertaining to the incident stream
$(\ )_2$ = pertaining to the target stream
$(\ )_3$ = pertaining to a participating excited state

Received May 28, 1974; revision received October 24, 1974. This work was sponsored by the Advanced Research Projects Agency, ARPA Order No. 1857, Contract F04611-72-C-0035. The technical monitor of the work was the Air Force Rocket Propulsion Laboratory, Edwards Air Force Base, California. A more extensive discussion of the details of the experiment are available in a report by the same authors and title, AFRPL-TR-74-30, July 1974.

Index category: Thermochemistry and Chemical Kinetics.

* Principal Engineer, Aerodynamic Research Department. Member AIAA.

† Principal Engineer, Aerodynamic Research Department.

‡ Head, Aerodynamic Research Department. Associate Fellow AIAA.

I. Introduction

THE experiment that is described here was designed to determine the transition probability for vibrational excitation of molecules excited in a single high-energy collision. These transition probabilities have previously been inferred from vibrational relaxation experiments, where a distribution of collisional energies is involved, rather than from monoenergetic collisions. For the experiments discussed here, a pressure-driven reflected-shock tunnel was used to produce N_2 molecules at a velocity of 5.8 km/sec, O atoms at 4.3 km/sec, or argon at 5.4 km/sec at sufficiently low density that the effect of single collisions could be observed. A liquid-nitrogen cooled flat plate containing a gas injector was aligned with the flow in the test section, and used to inject target gases of H_2O, CO_2, or NH_3. A Ge:Hg infrared detector was located in this plate downstream of the injector to observe infrared radiation from the collisionally excited molecules. A second flat plate, also cooled with liquid nitrogen, was placed parallel to the first plate and served as a cooled background for the detector.

For the experimental arrangement just described, the energy transferred to internal excitation of the target molecule is close to the maximum for this type of collision. Viewed in the center-of-mass coordinate system, such a collision results in both particles emerging from the interaction zone with little residual velocity. In the laboratory system both particles, and in particular the excited target molecule, move with a velocity close to that of the center of mass. Since the initial velocity of the target molecule is an order of magnitude smaller than the approaching N_2 molecule, O atom, or argon, the center-of-mass velocity is approximately aligned with the velocity of the N_2, O, or argon stream. Thus the excited target molecules travel downstream nearly parallel to the direction of the bombarding stream.

One can take advantage of this special feature of these collisions to design an experiment in which excited states are generated at one streamwise location and the associated radiation intensity is viewed by an infrared detector at a location farther downstream. The design limitations, then, are related to the lifetime of the excited state as compared with the transit time to

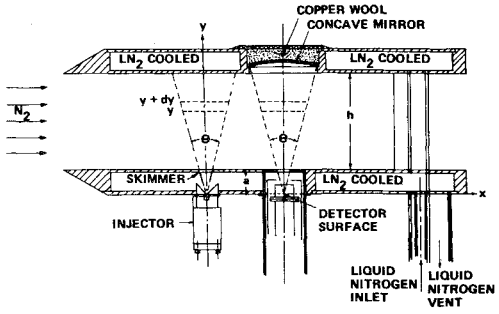

Fig. 1 Schematic of the experiment.

(and through) the field of view of the detector, and to the probability of collisional de-excitation.

In Sec. II, the experimental apparatus and diagnostic techniques used to obtain these results are described. In Sec. III is discussed the data reduction procedure used to convert the detector output to the appropriate values of (σ_*/τ) and in Sec. IV, the theoretical calculations utilized to go from values of (σ_*/τ) to values for the excitation cross section σ_*. The experimental data are presented in Sec. V for the interaction of N_2-H_2O, N_2-CO_2, N_2-NH_3, O-H_2O, and Ar-H_2O.

II. Experimental Apparatus and Technique

A. Shock-Tunnel Measurements

The shock-tunnel used in this work utilizes a 3-in. internal diam by 42 ft long pressure-driven shock tube as its gas supply. For the nitrogen experiments the driver gas was hydrogen at 10,000 psi and 670 K, and the driven-gas initial pressure was 30 torr and room temperature. For the oxygen experiments the driver gas was helium at 12,000 psi and 670 K, and the driven-gas initial pressure was 30 torr and room temperature. For the argon experiments the driver gas was hydrogen at 12,000 psi and 670 K, and the driven-gas initial pressure was 30 torr. Flow is initiated by rupturing the double diaphragms which initially separate the driver and driven gases. The flat-plate model used in this work is shown in Fig. 1 and was located on the centerline just downstream of the 6 ft diam nozzle exit plane.

Because of the high-enthalpy conditions of interest in this study, it was known that the available test time would be relatively small. It was felt to be essential to the success of the study that the duration and uniformity of the test-gas flow be determined experimentally. Therefore, several diagnostic experiments were performed for the shock-tube flow and for the nozzle flow in order to define the parameters of interest. A detailed discussion of these measurements is presented in the final report referred to in the footnote.

B. Detector and Filter Calibration

The infrared detector used in these experiments was a liquid helium cooled mercury-doped germanium detector. The field of view of the detector was terminated at the opposite wall of the model by a surface-silvered spherical mirror whose center of curvature was approximately coincident with the detector chip. The purpose of this mirror was to minimize diffused reflection of radiation into the detector, which could have occurred since the LN_2-cooled model was suspended in a vacuum tank at room temperature. Provided the surface of the mirror did not frost, the only background radiation that could enter the detector, in principle, had to come from the surface of the mirror. The mirror was backed by a pad of copper mesh to keep it in good thermal contact with the LN_2-cooled model.

For these experiments, the radiation intensity was observed in the region from 2.5–14.0 μm using eight different filters. The half-power points for each of these filters are: a) 2.5–3.1 μm, b) 4.28–4.34 μm, c) 5.7–7.5 μm, d) 8.3–9.2 μm, e) 8.3–14.0 μm, f) 9.1–10.3 μm, g) 10.6–11.6 μm, and h) 11.1–14.0 μm. The field of view of the detector is 30° and a 2-mm-thick Irtran 2 window, cooled to liquid nitrogen temperature, separates the detector shroud from the test flow. For each experiment, one of these eight filters, cooled to near liquid helium temperature, is placed between the detector and the Irtran 2 window in the field of view. It was therefore necessary to perform calibration experiments for each of the filters by employing a known input radiant flux of the same order as expected in the experiment. This input signal was provided by a platinum wire, 0.0001 in. diam by 0.100 in. long, placed in the FOV and electrically heated to provide the necessary radiant flux. By measuring the wire resistance and knowing the spectral emissivity[1] of platinum as a function of temperature, it was possible to calculate the radiant flux emitted by the wire over each bandwidth. A detailed discussion of the calibration technique is also presented in the final report.

C. Measurement of Injected-Gas Flow Rates

The number of target molecules, n_2, entering the path of the incident stream and the velocity, v_2, of these target molecules must be known in order to deduce values of σ_*/τ from the experimental results. A brief description of the data reduction procedure and the importance of these parameters can be found in Sec. III. The purpose of this discussion is to describe the experimental techniques used to obtain the values appropriate to these experiments.

To determine the H_2O, CO_2, or NH_3 particle density and time history, an ionizer built in the form of a cube was placed flush with the plate surface at the outlet of the injector. The opening into the ionizer was just slightly larger in diameter than the injector outlet. A beam of 80 ev electrons was established in the ionizer and the injector was operated. This permitted the target gas to flow and the collected ion and electron currents were monitored on an oscilloscope. In order to convert the measured ion current to particle density, the ionizer was filled with a known density of air molecules and the current measured. Knowing the ionization cross sections[2,3] as a function of electron energy for all of the species involved, the H_2O, CO_2, and NH_3 particle densities were determined at the location $(a+l)$ where (a) is the distance between the x-axis and the plate surface and (l) is the ionizer length. The inverse square law can then be used to determine the particle density at the plate surface using a straightforward calculation.

The velocity of the target molecules, v_2, was calculated from the expression $v_2 = (2/\gamma - 1)^{1/2}/a_0$ where a_0 is the speed of sound in the injector reservoir. In order to ascertain a_0, it was necessary to measure the temperature of the gas in the injector when the plates were cooled to liquid nitrogen temperature. To make this measurement, a platinum wire 0.0001 in. diam and 0.10 in. long was supported between two needles and placed in the injector chamber. The temperature coefficient of resistivity of platinum is well known but was independently checked (from room temperature to 77 K). By measuring the wire resistance at room temperature and after the plates had reached a steady-state temperature, it was possible to infer the injector gas temperature and thus a_0. The water vapor, which was in equilibrium with the liquid in the reservoir, was found to be at a temperature of 343 K higher than either the CO_2 or NH_3 vapor temperature because hot water was circulated through the injector jacket for the H_2O experiments but not for the CO_2 or NH_3 experiments. The corresponding reservoir pressure would have been 220 torr. However, the injector nozzle was cooled by contact with the liquid-nitrogen cooled flat-plate model. Thus the effective pressure was significantly less. The target gas was expanded rapidly from this reservoir condition in a nozzle with a length of 0.38-in. and an included angle of 90°. A liquid-nitrogen cooled skimmer was located downstream of the nozzle exit plane at the surface of the flat-plate model. It is anticipated that the water molecules striking the nozzle walls would be frozen-out. Condensation of the target-gas stream is not anticipated because of the rapid expansion in the short

nozzle with the walls cooled to 77 K. It is a difficult task to calculate accurately the target-gas particle density for the flow conditions of interest here. Thus the target-gas density was measured using an ionizer as explained above.

The temperature of the CO_2 vapor was measured to be 217 K at a pressure of 45 torr, and for the NH_3 vapor the measured temperature was 215 K at a pressure of 45 torr. The appropriate values of the specific heat ratio were taken from Ref. 4 for H_2O and CO_2 and from Ref. 5 for NH_3. The accuracy of the ionizer measurements of target-gas densities depends, in addition to the ionization cross-section data used, on the assumption that the target stream is uniform. The ionization cross-section data are considered to be accurate to within $\pm 20\%$ and it is estimated that stream nonuniformities would not introduce more than a few percent error in the calibration. Thus the overall density measurement of the target stream is considered to be accurate to within about 30%.

III. Elementary Theory of the Infrared Measurements

The theory of the infrared measurements reported here is based on the approximation that the excited target molecules, whose radiation was observed, traveled from their point of excitation parallel to the x-axis at the center-of-mass velocity, v_*. It is assumed that the lifetime τ of any participating state is long compared with the transit time to, and through, the field of view. A cross section σ_* is assigned to each excitation of interest.

The schematic of the experiment is shown in Fig. 1. The x-axis lies a distance (a) below the surface of the lower plate, and passes through the effective origin of the target-gas stream and through the apex of the field of view, both of which are conical with the same apex angle, θ. The target stream is attenuated by collisions with the high-speed N_2, O, or Ar stream, and essentially vanishes before reaching the upper plate. These collisions are primarily elastic, involving the normal gas-dynamic cross section, σ_0. It is tacitly assumed that the cross sections for exciting the states of interest in these experiments σ_* are at least an order of magnitude smaller than the gas-dynamic cross section. Thus the production of excited states does not affect the distribution of target molecules.

The total photon flux into the detector can be calculated on the basis of certain assumptions, namely that both streams of particles are essentially monoenergetic, that the excited species moves essentially parallel to the lower plate at the center-of-mass velocity, and that there is some effective excitation cross section σ_* for the participating states together with a radiative lifetime τ for these states.

It can be shown that the total photon flux into the detector is given by

$$w = \int_a^h \int_0^{y\tan(\theta/2)} \frac{A_d n_1 \sigma_* v_1 \psi_2(y)}{2\pi^2 v_* \tau v_2 y^4 \tan^2(\theta/2)} [y^2 \tan^2(\theta/2) - z^2] dz\, dy = \frac{A_d n_1 \sigma_* v_1}{\pi^2 v_* \tau v_2 \tan^2(\theta/2)} \int_a^h \psi_2(y) \left[\frac{\tan^3(\theta/2)}{y} - \frac{\tan^3(\theta/2)}{3y}\right] dy = \frac{A_d n_1 \sigma_* v_1}{\pi^2 v_* \tau v_2} \frac{4}{3} \tan(\theta/2) \int_a^h \frac{\psi_2(y)}{y} dy \quad (1)$$

It is consistent to make the approximation that $\tan\theta/2 \cong \theta/2$, and since $\psi_2(y) \cong 0$ for $y \leqq h$, Eq. (1) can be written

$$w = \frac{2A_d \theta n_1 v_1}{3\pi^2 v_* v_2} \left(\frac{\sigma_*}{\tau}\right) \int_a^\infty \frac{\psi_2(y)}{y} dy \quad (2)$$

where the dependence of the number of photons/sec, w on the ratio σ_*/τ is shown explicitly.

An expression can be derived for $\psi_2(y)$ and when substituted into Eq. (2), the number of photons/sec entering the detector is given by

$$w = \frac{2A_d \theta n_1 v_1}{3\pi^2 v_* v_2} \left(\frac{\sigma_*}{\tau}\right) \psi_2(a)\, e^{a/\eta} \int_a^\infty \frac{1}{y} e^{-y/\eta} dy \quad (3)$$

Putting $\xi = y/\eta$, Eq. (3) can be written in terms of a tabulated integral

$$w = \frac{2A_d \theta n_1 v_1}{3\pi^2 v_* v_2} \left(\frac{\sigma_*}{\tau}\right) \psi_2(a)\, e^{a/\eta} \int_{a/\eta}^\infty \frac{1}{\xi} e^{-\xi} d\xi \quad (4)$$

The total flux of target molecules at the surface of the lower plate $\psi_2(a)$ can be expressed in terms of the probability P that an N_2 molecule will collide with a target molecule in traversing the maximum path length (diameter) in the target stream at $y = a$. Writing $n_2(y)$ for the density of target molecules, to an approximation consistent with Eq. (4),

$$\frac{P}{\sigma_0} = 2a \tan(\theta/2) n_2(a) \quad (5)$$

And since

$$\psi_2(a) = \pi a^2 \tan^2(\theta/2) v_2 n_2(a) \quad (6)$$

this becomes

$$\psi_2(a) = \frac{\pi a v_2}{2} \left(\frac{P}{\sigma_0}\right) \tan(\theta/2) \quad (7)$$

Finally, to the same approximation as Eq. (4), the total number of photons/sec entering the detector is given by

$$w = \frac{A_d \theta^2 n_1 v_1 a}{6\pi v_*} \left(\frac{P}{\sigma_0}\right) \left(\frac{\sigma_*}{\tau}\right) e^{a/\eta} \int_{a/\eta}^\infty \frac{1}{\xi} e^{-\xi} d\xi \quad (8)$$

which, when multiplied by the energy/photon becomes the wattage into the detector attributable to the excitation corresponding to σ_*. The value of σ_0 used in Eq. (8) to deduce the values of σ_*/τ (reported in Tables 1–4 and 6–8) from the measured photon flux were: 3.22×10^{-15} cm^2 for N_2-H_2O; 4.54×10^{-15} cm^2 for N_2-CO_2; 1.7×10^{-15} cm^2 for N_2-NH_3; 2.7×10^{-15} cm^2 for O-H_2O; and 2.5×10^{-15} cm^2 for Ar-H_2O. For the comparison presented in Table 5 and in Sec. VH, the value used for σ_0 was 1.15×10^{-15} cm^2 to be consistent with the theoretical calculation.[6]

Table 1 Experimental results for N_2-H_2O at 5.8 km/sec

Filter microns	No H_2O injection photons/sec	With H_2O injection photons/sec	Signal due to H_2O photons/sec	$(\sigma_*/\tau)_{exp}$ cm^2 sec^{-1}
2.5–3.1	9.9×10^9	9.3×10^9	$< 0.95 \times 10^9$	$< 0.037 \times 10^{-15}$
5.7–7.5	1.9×10^{10}	3.1×10^{10}	1.2×10^{10}	0.46×10^{-15}
8.3–9.2	1.0×10^9	1.9×10^9	0.9×10^9	0.035×10^{-15}
9.1–10.3	1.0×10^9	2.1×10^9	1.1×10^9	0.042×10^{-15}
10.6–11.6	2.4×10^9	4.8×10^9	2.4×10^9	0.092×10^{-15}
11.1–14.0	1.5×10^{10}	1.9×10^{10}	4.0×10^9	0.15×10^{-15}
8.3–14.0	5.7×10^9	1.5×10^{10}	0.9×10^{10}	0.35×10^{-15}

Table 2 Experimental results for N_2-CO_2 at 5.8 km/sec

Filter microns	No CO_2 injection photons/sec	With CO_2 injection photons/sec	Signal due to CO_2 photons/sec	$(\sigma_*/\tau)_{exp}$ cm^2 sec^{-1}
4.28–4.34	7.8×10^8	9.5×10^8	0.17×10^9	0.007×10^{-15}
8.3–9.2	1.0×10^9	1.3×10^9	0.3×10^9	0.012×10^{-15}
9.1–10.3	1.0×10^9	1.5×10^9	0.5×10^9	0.020×10^{-15}
10.6–11.6	1.6×10^9	1.7×10^9	0.1×10^9	0.004×10^{-15}
8.3–14.0	5.7×10^9	1.6×10^{10}	1.0×10^{10}	0.40×10^{-15}

Table 3 Experimental results for N_2-NH_3 at 5.8 km/sec

Filter microns	No NH_3 injection photons/sec	With NH_3 injection photons/sec	Signal due to NH_3 photons/sec	$(\sigma_*/\tau)_{exp}$ cm^2 sec^{-1}
8.3–9.2	1.0×10^9	3.9×10^9	2.9×10^9	0.079×10^{-15}
10.6–11.6	1.6×10^9	6.6×10^9	5.0×10^9	0.14×10^{-15}
8.3–14.0	5.7×10^9	2.5×10^{10}	1.9×10^{10}	0.51×10^{-15}

Table 4 Comparison of experimental results with calculations for N_2-H_2O at 5.8 km/sec

Energy interval cm^{-1}	$(\sigma_*/\tau)_{\Delta E}(f)$ cm^2 $sec^{-1} \times 10^{18}$ 5.67–7.45 μm	8.29–9.23 μm	9.13–10.33 μm	10.61–11.57 μm	11.05–14 μm	8.32–14 μm
0–770	0	0	0	0	0	0
770–1541	0	0	0	0	0	0
1541–2312	0	0	0	0	0.37	0.37
2312–3083	0	0	0	0.33	10.97	11.01
3083–3853	0	0	0.12	2.03	28.90	31.10
3853–4624	0	0.0018	2.16	7.34	35.27	48.17
4624–5395	0	2.11	6.41	10.90	30.68	54.10
5395–6166	0	6.30	11.62	21.60	31.00	66.03
6166–6936	0	9.56	14.28	22.41	232.57	281.28
6936–7707	1.37	12.03	32.20	4.94	673.30	710.86
7707–8478	1.24	9.48	21.74	12.55	767.74	802.82
8478–9249	7.30	13.35	252.53	10.11	477.40	748.55
9249–10019	25.81	4.72	161.86	1.06	273.00	442.65
10019–10790	30.49	2.08	89.59	50.58	130.63	221.49
10790–11561	0.76	0.95	31.33	33.02	84.46	137.16
11561–12332	53.65	0.08	14.80	18.49	40.56	103.93
12332–13105	30.08	0.21	17.41	49.98	26.31	75.39
13105–13873	106.48	19.13	9.18	21.27	9.39	76.07
13873–14644	0	0	0	0	0	0
14644–15415	0	0	0	0	0	0
$(\sigma_*/\tau)_{calc}(f)$	257.18	80.00	665.23	266.61	2852.55	3810.98
$(\sigma_*/\tau)_{exp}$	160.00	13.00	15.00	21.00	54.00	120.00
$(1/50)(\sigma_*/\tau)_{calc}$	5.00	1.6	13.00	5.3	57.00	76.00

Table 5 Cross sections for vibrational excitation in collisions with N_2 at 5.8 km/sec

	$\Delta\lambda$ μm	τ sec	$(\sigma_*/\tau)_{expt.}$ cm^2 sec^{-1}	$\sigma_*(\Delta\lambda)$ cm^2
H_2O 000–010	5.7–7.5	4.5×10^{-2}	0.46×10^{-15}	2.0×10^{-17}
000–001	2.5–3.1	2.5×10^{-2}	$<0.037 \times 10^{-15}$	$<9.3 \times 10^{-19}$
CO_2 000–010	11.6–14	4.3×10^{-1}	0.36×10^{-15}	1.6×10^{-16} (partial)
000–001	4.28–4.34	2.2×10^{-3}	0.007×10^{-15}	1.5×10^{-20} (partial)
NH_3 0000–0100	8.3–14	6.8×10^{-2}	0.51×10^{-15}	3.5×10^{-17}

The values pertaining to the actual experiments are:

$a = 2.54$ cm

$A_d = 0.0625$ cm^2

$n_1 = 2.75 \times 10^{14}$ cm^{-3} for 5.8 km/sec N_2 stream
$= 1.86 \times 10^{14}$ cm^{-3} for 4.3 km/sec O stream
$= 1.35 \times 10^{14}$ cm^{-3} for 5.4 km/sec Argon stream

$n_2(a) = 2.25 \times 10^{14}$ cm^{-3} (for H_2O)
$= 3.9 \times 10^{14}$ cm^{-3} (for CO_2)
$= 2.36 \times 10^{14}$ cm^{-3} (for NH_3)

$P/\sigma_0 = 0.31 \times 10^{15}$ cm^{-2} (for H_2O)
$= 0.53 \times 10^{15}$ cm^{-2} (for CO_2)
$= 0.32 \times 10^{15}$ cm^{-2} (for NH_3)

$v_1 = 5.8 \times 10^5$ cm/sec (for N_2-H_2O, N_2-CO_2, and N_2-NH_3)
$= 4.3 \times 10^5$ cm/sec (for O-H_2O)
$= 5.4 \times 10^5$ cm/sec (for Ar-H_2O)

$v_2 = 1.13 \times 10^5$ cm/sec (for H_2O)
$= 5.4 \times 10^4$ cm/sec (for CO_2)
$= 9.43 \times 10^4$ cm/sec (for NH_3)

$v_* = 3.53 \times 10^5$ cm/sec (for N_2-H_2O)
$= 2.26 \times 10^5$ cm/sec (for N_2-CO_2)
$= 3.61 \times 10^5$ cm/sec (for N_2-NH_3)
$= 2.02 \times 10^5$ cm/sec (for O-H_2O)
$= 3.70 \times 10^5$ cm/sec (for Ar-H_2O)

$\theta = 30°$ or 0.524 rad

$\sigma_0 = 3.22 \times 10^{-15}$ for N_2-H_2O
$= 4.54 \times 10^{-15}$ for N_2-CO_2
$= 1.7 \times 10^{-15}$ for N_2-NH_3
$= 2.7 \times 10^{-15}$ for O-H_2O
$= 2.5 \times 10^{-15}$ for Ar-H_2O

With these values, Eq. (19) can be used to express the experimental capability of measuring σ_*/τ in terms of the resolution of the detector.

$\sigma_*/\tau = 3.842 \times 10^{-26}$ (w) (for N_2-H_2O)
$= 4.036 \times 10^{-26}$ (w) (for N_2-CO_2)
$= 2.710 \times 10^{-26}$ (w) (for N_2-NH_3)
$= 2.012 \times 10^{-26}$ (w) (for O-H_2O)
$= 3.640 \times 10^{-26}$ (w) (for Ar-H_2O)

where w is in photons sec^{-1}.

The possibility of multiple collisions, which result in de-excitation of excited molecules, was a design consideration. This consideration leads to one of the design problems of the experiment which concerned the spacing of the target source and the detector. When operating with H_2O, the source is water-jacketed at approximately 340 K whereas the detector is at about 5 K and shielded at about 77 K. Therefore, adequate separation is necessary for thermal isolation. Also, in the flow between the plates, the cones of the target stream and of the field of view of the detector should not overlap up to a height beyond which essentially no excited states are produced. However, once a target

molecule is highly excited, it moves with the N_2 stream at a velocity $(v_1 - v_*)$ and its mean free path in the N_2 stream must be sufficient to ensure that collisional de-excitation will not interfere with the experiment. Thus the experiment was designed so that an excited molecule would have, on the average, about one collision before entering the detector field of view. The probability of de-excitation in a single collision is negligibly small.

The fraction F of the newly created excited particles that undergoes collision with N_2 particles (or O or Ar) can be estimated on the basis of the gas-dynamic collision cross section σ_0. The fraction of these excited particles that would suffer a collision in traveling the distance between position x_1 where the excited particle is formed to position x_2 where it would radiate in the FOV of the detector, is given by

$$F = 1 - \exp\left[- \frac{(x_2 - x_1)(v_1 - v_*)\sigma_0 n_1}{v_*} \right]$$

The collision between the excited particle and a N_2 molecule (or O atom or Ar) is a much lower energy collision than the initial collision between a N_2 particle and a target gas molecule. The distance between the centerline of the FOV of the target gas, x_1, and the centerline of the FOV of the detector, x_2, was approximately 3.7 cm for our experiments. Thus if we use the values of the gas-dynamic collision cross section σ_0 given previously, then we can estimate the fraction of the excited particles that undergo a collision in traveling the distance $x_2 - x_1$; for N_2-H_2O, $F = 0.88$; for N_2-CO_2, $F = 0.999$; for N_2-NH_3, $F = 0.65$; for O-H_2O, $F = 0.88$; for Ar-H_2O, $F = 0.44$.

From this calculation, it can be seen that for the N_2-H_2O and the O-H_2O experiments approximately 88% of the excited particles will undergo a collision with the incident particle. In the case of the N_2-NH_3 experiment, approximately 65% of the excited particles will experience a collision and in the case of the Ar-H_2O experiments 44% of the excited particles will undergo a collision with the incident particle. As previously noted, these second collisions are of much lower energy than the initial excitation collision and the probability for de-excitation is significantly less than it would be for a higher energy collision. It is thus doubtful that any significant de-excitation occurred for these collisions. However, in the case of the N_2-CO_2 experiment, 99.9% of the excited particles will undergo a second collision and this condition deviates significantly from our design consideration. There is a possibility that we may have had some de-excitation for the N_2-CO_2 experiment, even though the second collision was at much lower energy than the excitation collision. It is difficult for us to estimate the magnitude of this potential influence, but it can be seen that if de-excitation did occur then the reported values of σ_*/τ would be smaller than the true value.

The production of excited states which may contribute to the measured radiation is related to the ordinary gas-dynamic elastic collision cross section σ_0 by virtue of the fact that a change in σ_0 alters the geometrical location of the paths of the excited molecules with respect to the infrared optics. For example, an increase in σ_0 means that the water stream is attenuated more rapidly and the fraction of collisions that result in excited states occur closer to the source. Thus, they pass closer to the detector and spend less time in the field of view. It follows that the measured radiation is proportional to $(\sigma_*/\sigma_0)/\tau$ for the experimental condition under which few target particles reach the opposite wall. Thus, any experimental values determined for σ_* are proportional to the value assumed for σ_0, which is approximately a constant for any one experiment due to the fact that both streams are highly expanded and therefore nearly monoenergetic.

IV. Method of Data Analysis

Analysis of the data to determine the cross section for excitation has required an unfolding of the collisional excitation and radiative emission processes. For short wavelength vibrational transitions most of the emission occurs in a relatively small spectral range, and can be clearly identified as radiation from a specific excited vibrational state. The cross section for excitation of this state can then be determined by multiplying the experimental value of σ_*/τ by the known radiative lifetime for the transition. In this way the cross section for H_2O (000–010) at 6.3 μm and NH_3 (ν_2) at 10.7 μm were determined. For the other transitions, however, where the observed radiation originates from a broad range of energy levels, or where only a portion of the band was observed (as with CO_2), a somewhat more detailed analysis is required. This analysis was applied to the pure rotational spectrum of water, but has not been attempted for the CO_2 transitions. For the vibrational transitions it can be assumed that only the first vibrational level is excited. The probability of 2-quantum transitions is relatively small, since typical measured values of P_{01} are on the order of 0.025 or less, and probabilities of higher order transitions are related by[7] $P_{0n} = P_{01}^n(1/n!)$. For the rotational transitions, however, it is expected that multiple quantum jumps occur, and the classical treatment discussed herein is consistent with that.

A. General Formulation

The cross section for excitation to the v, R vibrational-rotational state is taken as

$$\sigma_{vR} = P_v P_R \sigma_0 \tag{9}$$

where P_v is a probability of excitation of a given vibrational state and P_R the probability of excitation of a given rotational state. For excitation to any given vibrational state v, the cross section is

$$\sigma_v = \sum_{\substack{\text{all} \\ R}} \sigma_{vR} = \sigma_0 P_v \sum_{\substack{\text{all} \\ R}} P_R = \sigma_0 P_v \tag{10}$$

where P_R is normalized so that

$$\sum_{\substack{\text{all} \\ R}} P_R = 1 \tag{11}$$

The intensity of the radiation that is observed immediately after collisional excitation is proportional to the ratio of the excitation cross section to the radiative lifetime, as previously discussed. Thus the parameter that can be measured for any transition j is

$$\bar{\theta}_j(v) = \sigma_{vR}/\tau_j = \sigma_{vR} A_j \tag{12}$$

where $A_j = 1/\tau_j$ is the Einstein coefficient for spontaneous emission, and τ_j is the lifetime for transition j, originating from level vR. Combining Eqs. (10) and (12) for pure vibrational transitions permits the simple data reduction discussed. In general, however, the filters employed transmit many spectral lines originating from considerably different energies, so that for each filter the observed radiation is proportional to the sum of all the terms $\theta_j(v)$ with values of v within the passband. Then for each filter f

$$\sigma_*/\tau(f) = \sum_{j(f)} \theta_j(v) = \sum_{j(f)} (\sigma_{vR} A_j) \tag{13}$$

or

$$\sigma_*/\tau(f) = \sigma_0 \sum_{j(f)} P_v P_R A_j \tag{14}$$

where $j(f)$ indicates all the spectral lines j passed by filter f.

Because of the large number of energy levels to which transitions can occur, compared with the relatively few passbands in which observations are made, it is necessary to make some assumption about the values of P_R and P_v, and then adjust these assumptions to obtain a consistent comparison with the data. To accomplish this, P_R is taken to depend only on the ratio of the energy of the rotational state to the center-of-mass energy of the collision. The energy dependence that is utilized is the calculated values obtained by Kolb et al.[6] for an impulsive rigid-rotor classical model of H_2O collisions with oxygen atoms. With this model the probability of excitation into an energy range E to $E + \Delta E$ is equal to $P\Delta E/E_{cm}$ so that $P(E/E_{cm})$ is normalized by the relation $\int_0^1 P(E/E_{cm})\, d(E/E_{cm}) = 1$. In the present usage the probability of excitation into an energy level i is equal to P_{R_i} so

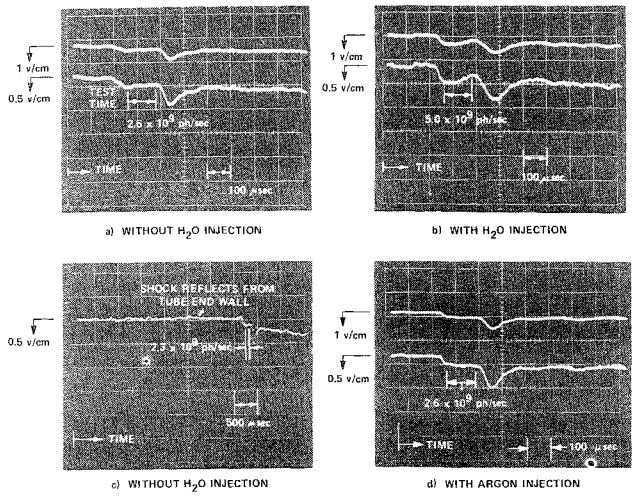

Fig. 2 Oscilloscope records obtained for 10.6–11.6μ filter for 5.8 km/sec N_2 particles.

that the normalization relation is $\sum_{i=1}^{i_{max}} P_{R_i} = 1$, where i represents the ith energy level and i_{max} is the total number of rotational levels considered. Thus Kolb et al. values are related to those used here by

$$P_{R_i} = CP(E) \tag{15}$$

where C is a single proportionately constant determined from $\sum_{i=1}^{i_{max}} P_{R_i} = 1$. (Since the energy levels are distributed with reasonably constant density in the energy range of interest, C is approximately given by $C = 1/i_{max}$.)

B. H_2O Rotation

The pure rotational spectrum of H_2O extends over the entire 8–14 μm infrared region of interest. The energies of the rotational states and the wavelength and intensities of the transitions which originate from them have been calculated by Maki[8] and these calculations have been used in the present data reduction. They show that the radiation of 14 μm wavelength or shorter originates from energy levels of $J \geqq 16$, or energies >5000 cm^{-1}. Thus, single-collision excitation of this radiation requires energetic collision. The calculation described by Eqs. (14) and (15), using Maki's values of A_j and Kolb's values of $P(E)$, is tabulated in Table 4 and compared with experiment.

V. Presentation of Experimental Data

A. N_2-H_2O Collisions at 5.8 km/sec

The experimental results obtained for the infrared radiation from H_2O collisionally excited by N_2 at 5.8 km/sec are given in Table 1 for all of the wavelength intervals studied in this work. Three important comments can be made about the results appearing in this table. First, the photon flux measured in the absence of H_2O injection for the 2.5–3.1 μm wavelength region was approximately equal to (6% greater) that measured with injection, suggesting that the H_2O stretching mode was not excited. On the basis of experience with these measurements we feel that 10% effects can be resolved and that the slight change in signal observed at this wavelength with H_2O injection is not significant. The data reported in Table 1 for this wavelength suggest that the value of σ_*/τ must be less than 3.7×10^{-17} cm^2 sec^{-1}. Secondly, the magnitude of σ_*/τ measured in the 5.7–7.5 μm region is relatively large (0.46×10^{-15} cm^2 sec^{-1}) and is roughly the same as the value measured over the entire 8.3–14 μm region (0.35×10^{-15} cm^2 sec^{-1}). Finally, the sum of the σ_*/τ values measured at the 8.3–9.2, 9.1–10.3, 10.6–11.6, and 11.1–14.0 μm wavelength intervals is approximately equal to the value of σ_*/τ measured with the 8.3–14.0 μm filter, as would be expected.

Figure 2 is typical of the data obtained in the nitrogen experiments. Figure 2(a) illustrates the detector-output history measured in the 10.6–11.6 μm wavelength region in the absence of H_2O injection. The test time is shown to be on the order of 100 μsec, consistent with the measurements discussed in Sec. II., and the photon flux is relatively uniform during this time period. Figure 2b was obtained for the same N_2 velocity but in this experiment H_2O was injected as a target gas. The photon flux measured during the test flow was almost a factor of two greater than that measured in the absence of H_2O injection.

Figure 2c is an oscilloscope record from a different "no injection" experiment, but this oscilloscope was triggered by a heat-transfer gage located 20 in. downstream from the driver-tube diaphragm and the scope sweep speed was 500 μsec/cm instead of 100 μsec/cm as used on Figs. 2a, 2b, and 2d. The reason for showing this record is to illustrate that when the incident-shock reflects from the driven-tube end wall, creating the reservoir of high-enthalpy particles, the detector does not receive a signal from the shock tube that could potentially influence the results.

To be sure that the increased signal observed when H_2O was injected could in fact be attributed to the N_2-H_2O interaction, several experiments were performed in which argon was injected instead of H_2O. Figure 2d illustrates that when argon was injected the recorded detector output was found to be nearly identical to the signal received in the absence of injection.

Figure 3 is another illustration of the experimental data obtained with and without H_2O injection. These particular oscilloscope records were obtained using the 8.3–14.0 μm filter. Figure 3a illustrates that the photon flux measured in the absence of H_2O injection was 6.0×10^9 ph/sec as compared to the value of 1.6×10^{10} ph/sec shown in Figure 3b which was measured with H_2O injection. These results are included in the data summary presented in Table 1 and, as indicated there, result in a value of σ_*/τ equal to 0.35×10^{-15} cm^2 sec^{-1} for this wavelength region.

B. N_2-CO_2 Collisions at 5.8 km/sec

The experimental results obtained for the infrared radiation from CO_2 collisionally excited by N_2 at 5.8 km/sec are given in Table 2 for all wavelength intervals studied in this work. One additional filter appears in this table (4.28–4.34 μm) not used in the N_2-H_2O work. In addition, the 5.7–7.5 μm and the 11.1–14.0 μm filters were not used in the N_2-CO_2 studies. It was difficult to excite the 4.28–4.34 μm mode, as illustrated by the fact that the signal received by the detector with CO_2 injection was only 15% greater than that received without injection. For wavelength intervals 8.3–9.2 μm, 9.1–10.3 μm, and 8.3–14.0 μm, the signals recorded with injection were considerably greater than the background signals. However, in the 10.6–11.6 μm region, the signals recorded with injection of CO_2 were less than 10% greater than those recorded in the absence of injection, so that only an upper limit of the value for σ_*/τ could be determined at this wavelength interval.

C. N_2-NH_3 Collisions at 5.8 km/sec

Table 3 presents a summary of the values for σ_*/τ obtained for N_2 particles at 5.8 km/sec interacting with NH_3. The three

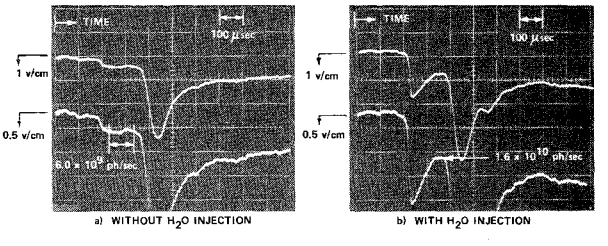

Fig. 3 Oscilloscope records obtained for 8.3–14.0μ filter for 5.8 km/sec N_2 particles.

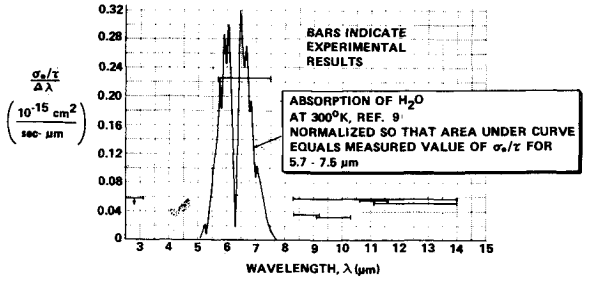

Fig. 4 Spectral dependence of collisionally induced radiation with H_2O-N_2 at 5.8 km/sec.

wavelength intervals that were studied for this combination of gases were 8.3–9.2 μm, 10.6–11.6 μm, and 8.3–14.0 μm. Even though all the available filters were not used in this study, the results presented in Table 3 suggest that the value of σ_*/τ measured for the 8.3–14.0 μm wavelength region is consistent with the values measured in the two intermediate wavelength intervals.

The photon flux recorded in the absence of injection was approximately 9.6×10^8 ph/sec. When CO_2 was injected, the photon flux increased to 1.3×10^9 ph/sec and the resulting σ_*/τ was deduced to be 0.012×10^{-15} cm^2 sec^{-1}. However, when NH_3 was injected, the photon flux increased to 4.0×10^9 ph/sec and the value of σ_*/τ was determined to be 0.079×10^{-15} cm^2 sec^{-1}.

Comparison of Tables 1–3 suggests that the values of σ_*/τ measured at selected wavelength intervals for N_2-NH_3 collisions were always greater than corresponding values measured for either the N_2-H_2O or N_2-CO_2 interactions. However, the N_2-CO_2 radiation in the 11.6–14 μm (i.e., near the 15 μm bending of CO_2) is probably greater than that for H_2O or NH_3. It can further be noted that the values of σ_*/τ measured at specified wavelength intervals for the N_2-H_2O interactions were generally greater than corresponding values measured for N_2-CO_2 interactions.

The spectral nature of the results is demonstrated in Figs. 4–6. On each graph, the quantity $(\sigma_*/\tau)/\Delta\lambda$ is plotted vs wavelength, and is compared with the optical absorption coefficient for the target gas. The shape of the absorption coefficients used were those for 300° gas. The purpose of the comparison is to demonstrate the correlation between the measured radiation and the spectral features of the gas, thus confirming that the source of radiation is the species being introduced through the target beam.

In Fig. 4, the absorption[9] of the bending mode of water occurs at 6.3 μm. The rotational spectrum observed at long wavelength does not appear in the cold absorption spectrum, since it results from transitions between very high energy levels; analysis of these transitions is discussed in the following section. As indicated in Table 4, most of the contribution from the 5.7–7.5 μm filter and some from the 8.3–9.2 μm filter were used to determine σ_* for the 010 transition.

In Fig. 5, the absorption[10] curve of CO_2 is shown, the prominent features being the 4.3 μ asymmetric stretch and the 15 μ bending mode. The five measurements of $(\sigma_*/\tau)/\Delta\lambda$ are also shown. The measurement from 8.3–14 μm, corrected for the small contributions from 8.3–11.6, is plotted in the region 11.6–14 μm. It can be inferred from these figures that the measurement of σ_*/τ for both of these bands supply only partial measurements of σ_* for the (001) and (010) excitation cross sections.

In Fig. 6, the overall measurement of σ_*/τ from 8–14 μm for NH_3[11] has been used to normalize the scale of the curve. The separate measurements in the spectral region 8.3–9.2 μm and 10.6–11.6 μm are then plotted in their spectral regions and it is seen that they are consistent with the broad-band measurement. It is expected that the overall measurement from 8–14 μm supplies a good total cross section for excitation of the mode.

D. Rotational Data for N_2-H_2O Collisions

The ratio of excitation cross section to radiative lifetime for the pure rotational spectrum of H_2O was calculated as described in Sec. IV. The cross section σ_* used in that calculation was chosen for H_2O-O collisions and the present experiments should determine the scaling factor required for H_2O-N_2 collisions. The numerical results obtained for $\sigma_*/\tau(f)$ [Eq. (14)] for each energy interval and for each filter is shown in Table 4. The sum of these values over all energy intervals then supplies the value of $\sigma_*/\tau(f)$ to compare with experimental results $[(\sigma_*/\tau)_{EXPT.}]$. For this comparison, shown in Table 4, a value of $\sigma_0 = 1.15 \times 10^{-15}$ cm^2 was used to reduce the experimental data. This was done to be consistent with the value used by Kolb et al.[6] in obtaining $P(E/E_{cm})$, which was used in Eqs. (14) and (15). For this reason, the results of Table 4 are about three times less than those of Table 1. (See discussion Sec. III. concerning dependence of σ_* or σ_0.) It can be seen from Table 4 that the calculated values $[(\sigma_*/\tau)_{CALC}]$ are about 50 times too large at the long wavelengths, where there should be no interference from vibration-rotation transitions. In the third summary line of Table 4, the calculated value is shown reduced by a factor of 50. This brings the longer wavelengths into reasonable agreement, and the additional radiation at the short wavelength is attributable to the 000–010 vibrational-rotational transition. It would be concluded that σ_*/τ for rotational excitation of H_2O by N_2 is about 50 times less than that calculated by Kolb et al.[6] for excitation of H_2O by O atoms of the same energy. There is an unexplained discrepancy for the 10.6 μ–11.57 μ filter, where the low calculated value reflects the unusually small number of strong lines attributed to this wavelength region.

E. Vibrational Data for N_2-H_2O Collisions

The short-wavelength radiation at 5.67–7.45 μm has been attributed to the 000–010 vibrational-rotational transitions.

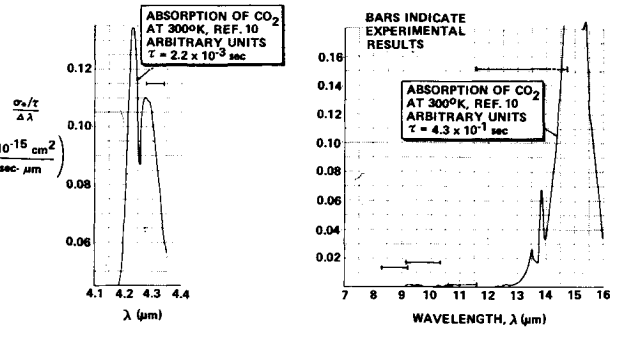

Fig. 5 Spectral dependence of collisionally induced radiation with CO_2-N_2 at 5.8 km/sec.

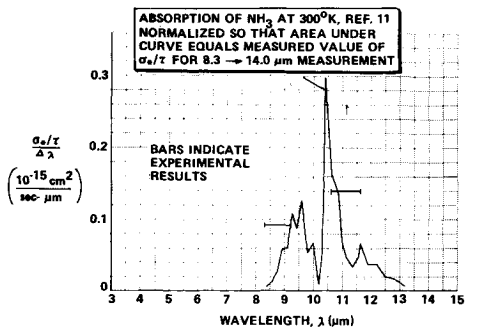

Fig. 6 Spectral dependence of collisionally induced radiation with NH_3-N_2 at 5.8 km/sec.

Using a lifetime of $\tau = 4.5 \times 10^{-2}$ sec[12], we obtain $\sigma_* = 2.1 \times 10^{-17}$ cm^2. A measurement in the wavelength interval 2.5–3.1 μm did not yield a measurable signal, and from this it was concluded that the cross section for the transition 000–001 is less than 9.3×10^{-19} cm^2. These data are summarized in Table 5.

F. Vibrational Data for CO_2 and NH_3 Excited by N_2 Collisions

Using a lifetime of 2.2×10^{-3} sec,[12] a measurement of CO_2 radiation with a narrow-band filter at 4.28–4.34 μm yields a partial cross section for excitation of (001) of CO_2 of 1.5×10^{-20} cm^2. This low value is associated with the narrow passband, as seen on Fig. 5. It is expected that measurement of all the radiation from this band would yield a cross section several times larger.

As seen in Table 2 and Fig. 5, most of the CO_2 radiation measured in the long-wavelength region is contained in 11.5–14.0 μm region. The wavelength of detector cutoff is nominally 14.0 μm at which point the sensitivity has decreased to 0.24 of maximum sensitivity. At 14.5 μm, the sensitivity has decreased to 0.1 of the 14.0 μm value, and at 14.75 μm, it has decreased to 0.05 of the 14.0 μm value.§ In Fig. 5, it is seen that the CO_2 transition probability increases by a factor of approximately 5 in the 14.0–14.5 μm interval and by a factor of approximately 10 in the 14.0–14.75 μm interval. It is probable that in these experiments a significant portion of the CO_2 radiation in the 14.0–14.75 μm region was received by the detector. For this reason, a dotted line has been used to represent that portion of the experimental result on Fig. 5 that extends beyond nominal detector cutoff.

The experimental determination of σ_* for the 000–010 transition, shown in Table 5 to be 0.16×10^{-15} cm^2 for a lifetime of 4.3×10^{-1} sec,[12] would represent a small fraction of the total cross section, but it is difficult to estimate the magnitude of this fraction. A recent calculation by R. Marriott[13] gives a value of $\sigma_* = 0.155 \times 10^{-15}$ cm^2 for collision at a relative velocity of 5.3 km/sec.

The NH_3-N_2 measurement utilized a filter which passed 8.3–14 μm. Separate measurements were made in the wavelength intervals 8.2–9.2 μm and 10.6–11.6 μm as shown in Table 3. As illustrated in Fig. 8, the region of interest is centered at about 10.4 μm so that the measurement from 8–14 μm should encompass the entire band. Using a radiative lifetime of 6.8×10^{-2} sec,[14] the corresponding value of σ_* can be calculated from the experimental data to be equal to 3.5×10^{-17} cm^2, which should properly represent the cross section for exciting the v_2 mode.

G. O-H_2O Collisions at 4.3 km/sec

The experimental results obtained for the infrared radiation from H_2O collisionally excited by O atoms at 4.3 km/sec are given in Table 6 for the wavelength intervals 2.46–3.13 μm, 5.67–7.45 μm, and 11.1–14.0 μm. It is difficult to compare these results directly with the N_2-H_2O results given in Table 1 because of the significant difference (4.3 km/sec vs 5.8 km/sec) in the O and N_2 particle velocities. These particle velocities are not the same because helium instead of hydrogen was used as the driver gas for the O-H_2O experiments since it was found that the H_2-O_2 interaction in the reflected-shock reservoir and in the nozzle expansion resulted in additional infrared radiation which would have significantly complicated interpretation of the results.

Table 6 Experimental results for O-H_2O at 4.3 km/sec

Filter microns	No H_2O injection photons/sec	With H_2O injection photons/sec	Signal due to H_2O photons/sec	$(\sigma_*/\tau)_{expt}$ cm^2 sec^{-1}
2.46–3.13	4.4×10^9	6.0×10^9	1.6×10^9	0.03×10^{-15}
5.67–7.45	9.5×10^9	15.0×10^9	5.5×10^9	0.11×10^{-15}
11.1–14.0	5.2×10^9	9.5×10^9	4.3×10^9	0.09×10^{-15}

§ Data supplied by Santa Barbara Research Corporation for the material from which this detector was cut.

H. Rotational Data for O-H_2O Collisions

The ratio of the excitation cross section to radiative lifetime for the pure rotational spectrum of H_2O was calculated for the oxygen experiments using the technique described in Sec. IV. Numerical results similar to those shown in Table 4 were obtained for each energy interval for the 11.1–14.0 μm filter. These values were summed over all energy intervals to arrive at a value of $(\sigma_*/\tau)_{CALC}$ which was approximately 1.4 times greater than the measured value $(\sigma_*/\tau)_{EXPT}$. The agreement between experiment and calculation suggests that the theoretical model[6] gives a correct description of the rotational excitation.

I. Vibrational Data for O-H_2O Collisions

Table 7 summarizes the short-wavelength radiation measurements obtained for the O-H_2O experiments. The 2.46–3.13 μm radiation has been attributed to the 000–001 H_2O stretching mode and the 5.67–7.45 μm radiation has been attributed to the 000–010 bending mode. Using radiative lifetimes of 2.5×10^{-2} sec and 4.5×10^{-2} sec, respectively, the excitation cross sections deduced from the experimental data are 7.5×10^{-19} cm^2 (2.46–3.13 μm) and 5.0×10^{-18} cm^2 (5.67–7.45 μm).

Table 7 Cross sections for vibrational excitation of H_2O in collisions with 0 atoms at 4.3 km/sec

	$\Delta\lambda$ microns	τ sec	$(\sigma_*/\tau)_{expt}$ cm^2 sec^{-1}	$\sigma_*(\Delta\lambda)$ cm^2
H_2O 000–010	5.67–7.45	4.5×10^{-2}	0.11×10^{-15}	5.0×10^{-18}
000–001	2.46–3.13	2.5×10^{-2}	0.03×10^{-15}	7.5×10^{-19}

J. Vibrational Data for Ar-H_2O Collisions

A limited number of experiments were performed in the 5.67–7.45 μm wavelength interval using argon at 5.4 km/sec colliding with H_2O as the target gas. The results of this study are reported in Table 8. Using a radiative lifetime of 4.5×10^{-2} sec for the H_2O 000–010 vibrational-rotational transition gives an excitation cross section of about 2×10^{-18} cm^2.

Table 8 Cross section for vibrational excitation of H_2O in collisions with argon at 5.4 km/sec

Filter microns	No H_2O injection photons/sec	With H_2O injection photons/sec	Signal due to H_2O photons/sec	$(\sigma_*/\tau)_{expt}$ cm^2 sec^{-1}	$\sigma_*(\Delta\lambda)$ cm^2
5.67–7.45	6.1×10^9	7.4×10^9	1.3×10^9	0.047×10^{-15}	2.1×10^{-18}

K. Comparison of Vibrational Cross Sections with Theory

Some estimate of the vibrational cross section to be expected can be obtained from comparison with the Milliken and White formulation of vibrational relaxation. This is discussed in the Appendix, and the results are shown in Table A1. These numbers can be compared with the experimental results in Table 5 for excitation by collision with N_2. The experimental results for these triatomic molecules do not agree well with the diatomic vibrational relaxation correlation of Millikan and White. If Eq. (A13) is evaluated for O-H_2O collisions at 4.3 km/sec. the resulting values of σ_* are 3.3×10^{-18} cm^2 for (000–010) and 1.4×10^{-20} cm^2 for (000–001). The experiments are close to agreement for (000–010) but indicate a much higher cross section for (000–001) than would be expected from the simple calculation.

VI. Conclusions

The spectral infrared radiative properties of H_2O, CO_2, and NH_3 molecules that have been involved in a single high-energy

Table A1 Millikan and White diatomic correlation applied to N_2 collisions with triatomic molecules

Collision partner	Vibrational transition	Energy cm^{-1}	Eq. (A3) A $°K^{1/3}$	Eq. (A3) B sec atm	Eq. (A2) $\sigma_0 K_1$ cm^2	Eq. (A2) K_2 cm sec^{-1}	σ_* for $v_1 = 5.2$ km sec^{-1} cm^2	σ_* for $v_1 = 5.8$ km sec^{-1} cm^2
H_2O	000–010	1595	1.16×10^{2}	4.24×10^{-10}	2.24×10^{-27}	1.88×10^{6}	1.6×10^{-17}	3.0×10^{-17}
	000–001	3755	3.64×10^{2}	4.85×10^{-13}	3.50×10^{-25}	1.04×10^{7}	1.9×10^{-22}	1.89×10^{-21}
CO_2	000–010	672	4.59×10^{1}	2.47×10^{-9}	3.0×10^{-27}	3.74×10^{5}	4.0×10^{-16}	5.3×10^{-16}
	000–001	2349	2.45×10^{2}	5.44×10^{-12}	1.13×10^{-25}	4.75×10^{6}	4.63×10^{-18}	1.43×10^{-17}
NH_3	0000–0100	932	5.58×10^{1}	2.21×10^{-9}	1.21×10^{-27}	6.36×10^{5}	9.7×10^{-17}	1.4×10^{-16}

collision with N_2, O, or argon have been measured. Experimentally determined values of excitation cross section/radiative lifetime (σ_*/τ) have been obtained for selected wavelength intervals for N_2-H_2O, N_2-CO_2, N_2-NH_3, O-H_2O, and Ar-H_2O collisions. These experimental values of σ_*/τ have been used in conjunction with available values of the radiative lifetimes for specific vibration-rotation transitions in order to calculate the appropriate values of the excitation cross section, σ_*. Using a Landau-Teller type of description of the collisions it was found that these results could be correlated with vibrational relaxation times for the different collision partners. The most difficult part of the data reduction procedure is that the deduced values of σ_*/τ are relatively sensitive to the value of the gas-dynamic cross section σ_0. Thus, we have provided sufficient information so that if improved values of σ_0 become available the σ_*/τ results could be appropriately corrected. The most sensitive steps in the experimental procedure were the calibration of the target-gas particle density and the calibration of the infrared detector. Considering the probable error for these measurements discussed in the paper we estimate that the overall accuracy of the σ_*/τ results is a factor of two.

Appendix A

Vibrational Data Correlation

The cross section for vibrational excitation as a function of impact velocity can be estimated by using collision theory in conjunction with measurements of vibrational relaxation. Collision theories yield that, for a collision between molecules which have an exponentially repulsive force, the probability of transition in a collision has the form

$$P_{10} = K_1 v^2 e^{-K_2/v} \tag{A1}$$

and the cross section σ_* for this transition is

$$\sigma_* = \sigma_0 P_{10} = \sigma_0 K_1 v^2 e^{-K_2/v} \tag{A2}$$

where σ_0 is the kinetic cross section. When the transition probability is averaged over a Boltzmann distribution of velocities, an expression for the vibrational relaxation time is obtained, of the form

$$p\tau = B e^{AT^{-1/3}} \tag{A3}$$

and this relation has considerable experimental confirmation. By following through the derivation (see, for example, Refs. 15 or 16) the constants in Eqs. (2) and (3) can be shown to be related by

$$K_2 = (2/3A)^{3/2}(k/\tilde{m})^{1/2} \tag{A4}$$

and

$$\sigma_0 K_1 = \frac{9}{32(2)^{1/2}} \frac{1}{N_0 T_0} \left(\frac{\tilde{m}}{k}\right)^{3/2} \frac{1}{BA^{3/2}} \tag{A5}$$

The units of $p\tau$ have been taken as atmosphere sec. T is the temperature in K, k is the Boltzmann constant, $\tilde{m}$ is the reduced mass of the colliding molecules, and N_0 and T_0 are the reference number density and temperature associated with the reference pressure of one atmosphere used in Eq. (A3). Thus $N_0 T_0 = 8.067\times10^{21}$ (particles/cm^3) K, and $(k/\tilde{m})^{1/2} = 1/(\mu)^{1/2}\ 9.117\times10^{3}$ $deg^{-1/2}$ cm/sec, where μ is the reduced molecular weight. Introducing these numbers, Eqs. (4) and (5) become

$$K_2 = 4962(A^3/\mu)^{1/2} \text{ cm/sec} \tag{A6}$$

$$\sigma_0 K_1 = 3.253\times10^{-35}(1/B)(\mu/A)^{3/2} \text{ sec}^2 \tag{A7}$$

and Eq. (2) is

$$\sigma_* = 3.253\times10^{-35} 1/B(\mu/A)^{3/2} v^2 e^{-4962(A^3/\mu)^{1/2}/v} \tag{A8}$$

The constants A and B can be obtained from vibrational relaxation data, in cases where these are available. Otherwise, estimates can be obtained from the semi-empirical correlation relations of Millikan and White.[17] From a comparison of 13 sets of collision partners, they obtain

$$A = c\mu^{1/2}\theta^{4/3} \tag{A9}$$

and

$$B = e^{-(0.015\mu^{1/4}A + 18.42)} \tag{A10}$$

where θ is the characteristic temperature $h\nu/k$ for the transition (in K) and c is a number close to 1.16×10^{-3}. Thus if the Millikan and White correlations are used, Eqs. (6) and (7) become

$$K_2 = 0.196\mu^{1/4}\theta^2 \tag{A11}$$

$$\sigma_0 K_1 = 8.228\times10^{-23}\mu^{3/4}\theta^{-2} e^{1.74\times10^{-5}\mu^{3/4}\theta^{4/3}} \tag{A12}$$

and Eq. (2) is

$$\sigma_* = 8.228\times10^{-23}\mu^{3/4}\theta^{-2} e^{1.74\times10^{-5}\mu^{3/4}\theta^{4/3}} v^2 e^{-(0.196\mu^{1/4}\theta^2)/v} \tag{A13}$$

With μ in molecular weight units, θ in K, and v in cm/sec, the cross section σ_* is in cm^2. The value of P_v to be associated with vibrational excitation in Eq. (21) is then σ_*/σ_0.

Values of the quantities in Eqs. (A9–A13) are given in Table A1 for the collisions of interest here. Experimental results of Simpson and Chandler[18] (also, see Ref. 19) give, for N_2-CO_2 (010) vibrational relaxation, $A = 38$ $K^{-1/3}$, $B = 5\times10^{-8}$ atm sec. These values, when used in Eq. (A8), give $\sigma_* = 4.0\times10^{-17}$ cm^2 for $v = 5.8\times10^{5}$ cm/sec.

References

[1] Rolling R. E., Funai, A. I., and Grammer, J. R., "Investigation of the Effect of Surface Condition on the Radiant Properties of Metals," TR 64-363, Nov. 1964, Air Force Materials Lab., Wright-Patterson Air Force Base, Ohio.

[2] Kieffer, L. J., "Compilation of Low Energy Electron Collision Cross Section Data Part I," Rept. 6, Jan. 1968, Joint Institute of Laboratory Astrophysics Information Center, University of Colorado, Boulder, Colo.

[3] Lampe, F. W., Franklin, J. L., and Field, F. N., "Cross Sections for Ionization by Electrons," *Journal of the American Chemical Society*, Vol. 79, Dec. 1957, pp. 6129–6132.

[4] Kennan, J. H. and Kaye, J., *Gas Tables*, Wiley, New York, 1945.

[5] Hodgman, C. D., editor, *Handbook of Chemistry and Physics*, 41st ed., Chemical Rubber Publishing Co., Cleveland, Ohio, 1959–1960, p. 2288.

[6] Kolb, C. E., Baum, H. R., and Tai, K. S., "Classical Calculations of H_2O Rotational Excitation in Energetic Atom-Molecule Collisions," *Journal of Chemical Physics*, Vol. 57, Oct. 1972, pp. 3409–3416.

[7] Treanor, C. E., "Transition Probabilities for the Forced Harmonic Oscillator," *Journal of Chemical Physics*, Vol. 44, Sept. 1966, pp. 2220–2221.

[8] Maki, A., Tables of Rotational Energy Levels and Transitions for H_2O, National Bureau of Standards, private communications.

[9] Brau, C. A., Lewis, P. L., Wu, P. K., and Young, L. A., "Plume Interference Assessment and Mitigation," AERL 73-1185, July 1973, AVCO Everett Research Lab., Everett, Mass.

[10] Burch, D. W., Gryvnak, D. S., Singleton, E. B., France, W. L., and Williams, D., "Infrared Absorption by Carbon Dioxide, Water Vapor, and Minor Atmospheric Constituents," AFCRL-62-698, July 1962, Air Force Cambridge Research Lab., Cambridge, Mass.

[11] "Plume Interference Assessment and Mitigation," Calspan Rept. No. K.C.-5134-A-3, Sec. II.2, Task II, Near-Field Analysis, Oct. 1972, AVCO Everett Research Laboratory, Everett, Mass., p. 12.

[12] Benedict, W. S. and Plyler, E. K., "High-Resolution Spectra of Hydrocarbon Flames in the Infrared," NBS Circular 523, March 1954, U.S. Dept. of Commerce, Washington, D.C., p. 64.

[13] Marriott, R., private communication, Research Institute for Engineering Sciences, Wayne State University, Detroit, Mich., Oct. 1973.

[14] Varanasi, P., "Shapes and Widths of Ammonia Lines Collision-Broadened by Hydrogen," *Abstracts of 27th Symposium on Molecular Structure and Spectroscopy*, Ohio State University, Columbus, Ohio, 1972.

[15] Schwartz, R. N., Slawsky, Z. I., and Herzfeld, K. F., "Calculation of Vibrational Relaxation Times in Gases," *Journal of Chemical Physics*, Vol. 20, 1952, pp. 1591–1597.

[16] Rapp, D. and Sharp, T. E., "Vibrational Energy Transfer in Molecular Collisions Involving Large Transition Probabilities," *Journal of Chemical Physics*, Vol. 38, Nov. 1963, pp. 2641–2648.

[17] Millikan, R. C., and White, D. R., "Systematics of Vibrational Relaxation," *Journal of Chemical Physics*, Vol. 39, Dec. 1963, pp. 3209–3213.

[18] Simpson, C. J. S. M. and Chandler, T. R. D., "A Shock Tube Study of Vibrational Relaxation in Pure CO_2 and Mixtures of CO_2 with the Inert Gases, Nitrogen, Deuterium and Hydrogen," *Proceedings of the Royal Society (London) Ser. A*, Vol. 317, 1970, pp. 265–277.

[19] Buchwald, M. I. and Bauer, S. H., "Vibrational Relaxation in CO_2 with Selected Collision Partners, I: H_2O and D_2O," *Journal of Physical Chemistry*, Vol. 76, Oct. 1972, pp. 3108–3115.

JUNE 1975 AIAA JOURNAL VOL. 13, NO. 6

On the Attitude Dynamics of Spinning Deformable Systems

J. C. SAMIN* AND P. Y. WILLEMS*
University of Louvain, Louvain-la-Neuve, Belgium

A general method for attitude dynamics investigation of spinning deformable systems is presented. The stability of given equilibrium configurations is determined by use of the Liapunov technique. Necessary and sufficient conditions are obtained in most cases. The choice of the body reference frame is considered, and the motion of various frames, such as principal axes frame, mean frame, and Tisserand's frame, is investigated.

Introduction

THE stability analysis of deformable mechanical systems is an important problem in applied mechanics and, in particular, for space technology applications. Many scientific papers have been devoted to this subject during the last decade, and realistic models have been presented even for sophisticated structures.

In a first approach to the rotational dynamics for nonrigid spacecrafts, the system is supposed to be a continuum, and its dynamical behavior is described by a set of ordinary and partial differential equations. Once an equilibrium configuration is defined, the attitude stability can be discussed from considerations on the linear displacements about that state and sufficient stability conditions can be obtained by various methods.[1-3]

Further, when the deformations are expressed in terms of a linear combination of normal modes, the behavior of the system can be described by a set of ordinary differential equations. Such an approach, introduced by Buckens in his pioneering work of 1963,[4] is very useful when the modal analysis is readily available but its applications are somewhat limited by the inevitable truncation problem.

The modelization as a continuum permits consideration of systems composed of various structures such as antenna's (booms, beams)[3,5,6] solar arrays (plates, shells),[7,8] fluid vessels, or any combination of these elements. As an example, Rumiantsev considered the rotational stability of systems, including rigid bodies, elastic parts, and cavities filled with (perfect) fluids.[9]

The multibody approach, or system discretization, is more directly oriented towards simulation but is also useful for stability investigation. Various formalisms have been developed and here Abzug's work seems to be a forerunner.[10,11] Hooker and Margulies considered a system of point connected rigid bodies and obtained vector dyadic equations expressed in terms of the angular variables corresponding to the relative motion between bodies.[12] Roberson and Wittenburg obtained independently equivalent matrix equations expressed in terms of the angular velocities of the bodies.[13] In both formalisms the torques acting in the connections were included, and the number of equations could have been larger than the number of degrees of freedom.

Hooker[14] suggested a procedure to eliminate unnecessary equations, and as suggested by Likins,[15] the equations obtained following Hooker's procedure and the Roberson-Wittenburg matrix formulation can be used for complex spacecraft simulation. A large number of computer programs were written using such ideas and simulation can then be obtained by direct integration of these nonlinear differential equations: this obviously limits the application to systems composed of a small number of equivalent rigid bodies, but appears to be very useful for a preliminary design. From that time onwards, the multibody formalism has been improved to include closed-loop configurations,[16] translations in the joints, effect of deformation, and rotors in the various bodies.[17-19]

Here also it must be noted that by an appropriate extension of Pringle's work,[20] necessary and sufficient stability conditions can be obtained from considerations on the Hamiltonian, and

Received February 11, 1974; revision received October 15, 1974. This research was partially supported by an "Aspirant" Fellowship from the F.N.R.S. (J. C. Samin) and carried out under ESRO Contract 2163/74AK.

Index category: Spacecraft Attitude Dynamics and Control.

* Department of Applied Mechanics (MEMA), University of Louvain.